

Fig. 1 Information exchange in nats from two-source (red line), single source (green and blue lines), and net synergy (black line) to target for linear, kraskov and kernel estimators. The error bars represents two standard deviations of the 100 permuted samples.

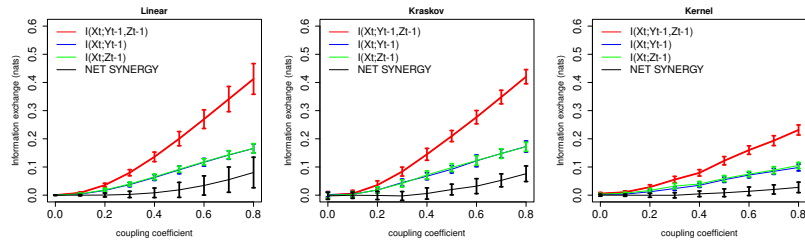


Fig. 2 Information exchange in nats from two-source (red line), single source (green and blue lines), net synergy (black line) to target for linear, kraskov and kernel estimators. The error bars represents two standard deviations of the 100 permuted samples.

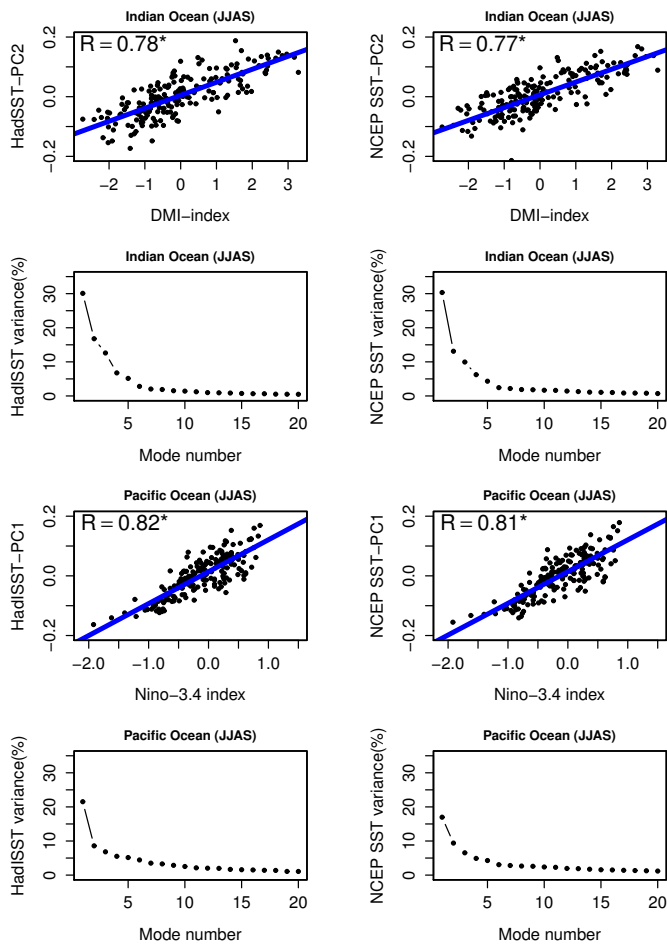


Fig. 3 Regressions of PCs obtained from their respective EOFs over the Indian and Pacific Oceans with the observed IOD and Niño 3.4 Index and their associated percentage contribution to the total variance for HadISST and NCEP reanalysis SST data sets.

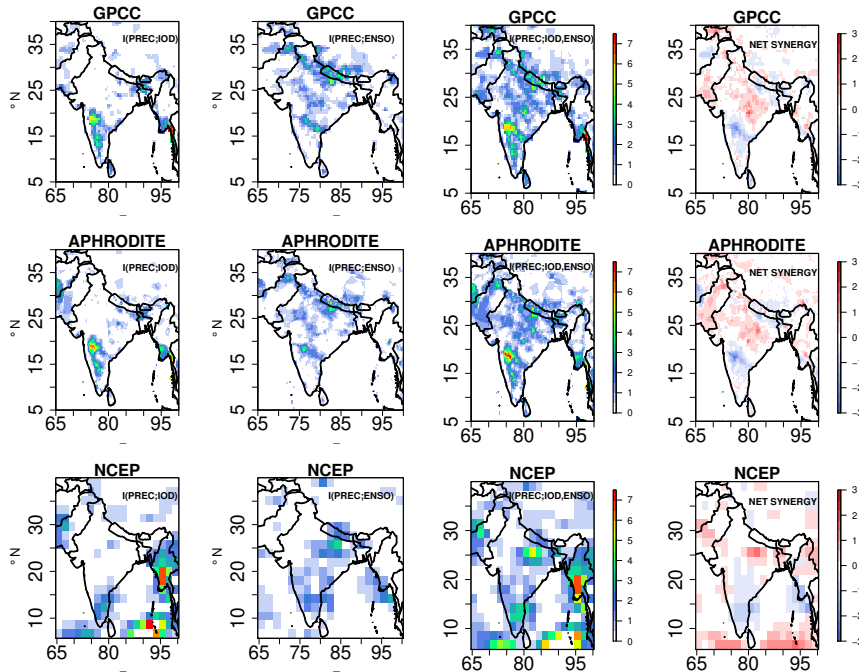


Fig. 4 Information exchange from $I(PREC;IOD)$, $I(PREC;ENSO)$, two-source information exchange $I(PREC; ENSO,IOD)$ and NET SYNERGY $\times 10^{-2}$ nats for observational data sets GPCC, APHRODITE and NCEP reanalysis with Kraskov estimator. Only significant values at 95% confidence intervals are plotted.

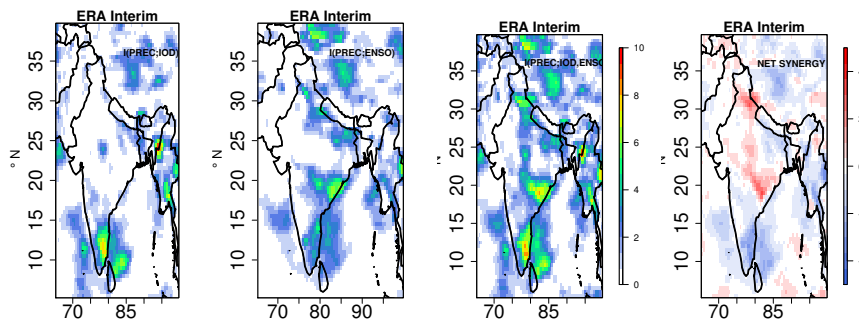


Fig. 5 Information exchange from $I(PREC;IOD)$, $I(PREC;ENSO)$, two-source information exchange $I(PREC; ENSO,IOD)$ and NET SYNERGY $\times 10^{-2}$ nats for observational data set ERA Interim reanalysis (1980-2005). Only significant values at 95% confidence intervals are plotted.

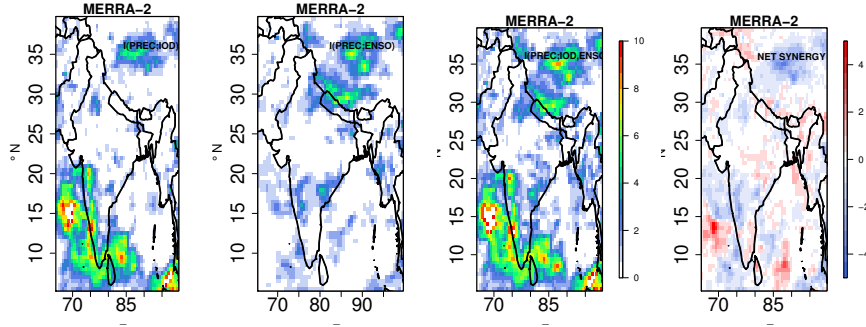


Fig. 6 Information exchange from $I(\text{PREC};\text{IOD})$, $I(\text{PREC};\text{ENSO})$, two-source information exchange $I(\text{PREC}; \text{ENSO},\text{IOD})$ and NET SYNERGY $\times 10^{-2}$ nats for observational data set MERRA-2 reanalysis (1980–2005). Only significant values at 95% confidence intervals are plotted.

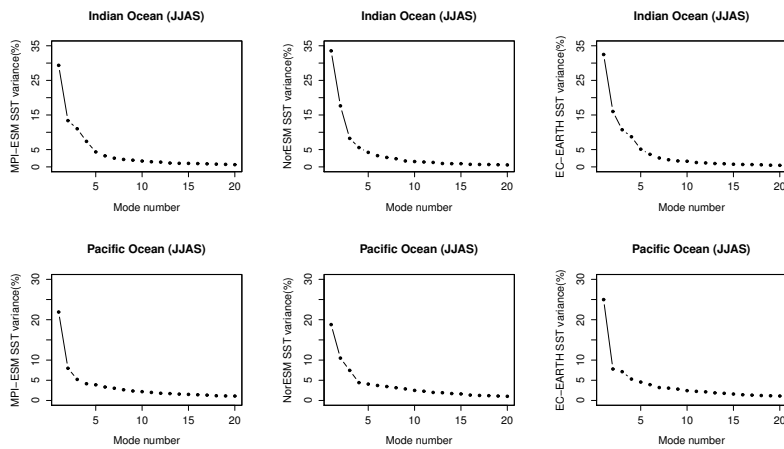


Fig. 7 Percentage of the total variance contributed by the first 20 EOFs to the total variability in Indian and Pacific Ocean SST for MPI-ESM-LR, Nor-ESM-M and EC-EARTH models for the month of JJAS (1951–2005)

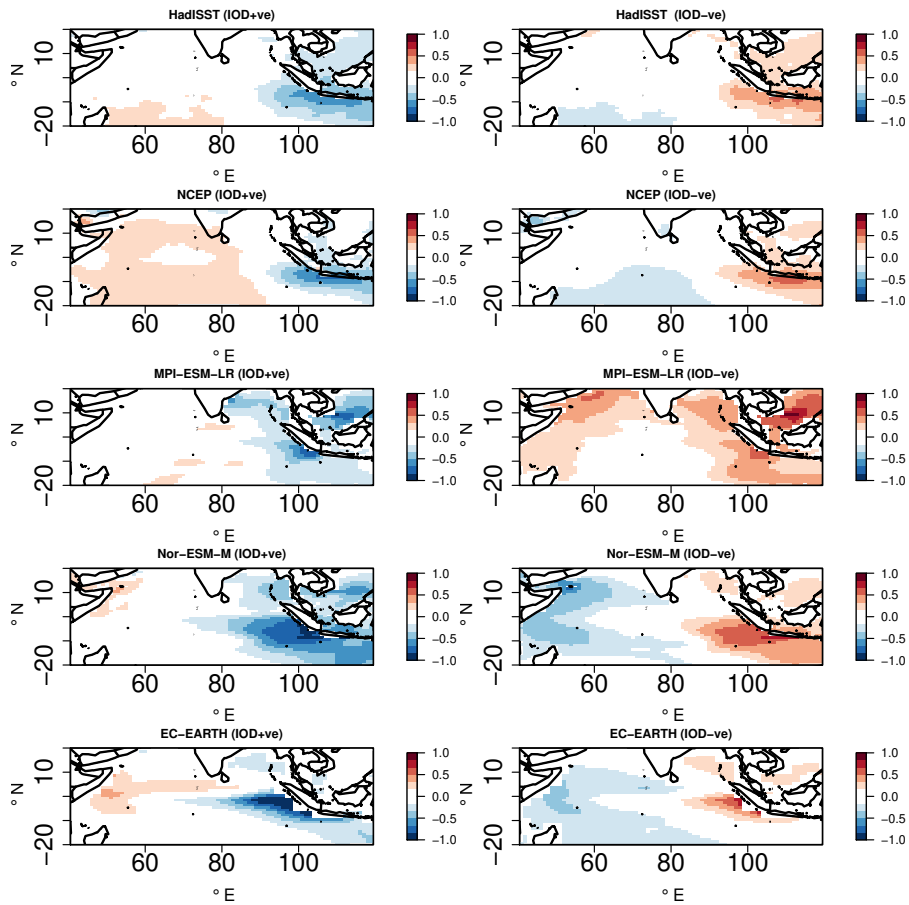


Fig. 8 SST composites for observations and GCMs for various phases of IOD events over the Indian ocean.

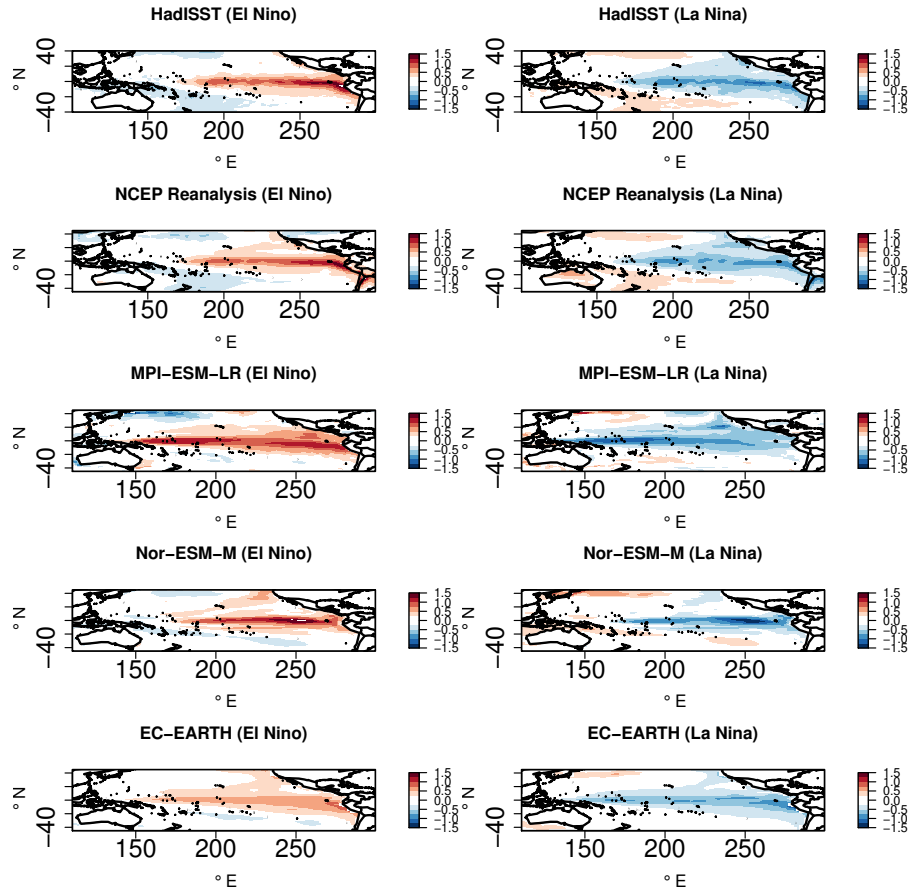


Fig. 9 SST composites for observations and GCMs for various phases of ENSO events over the Pacific ocean.

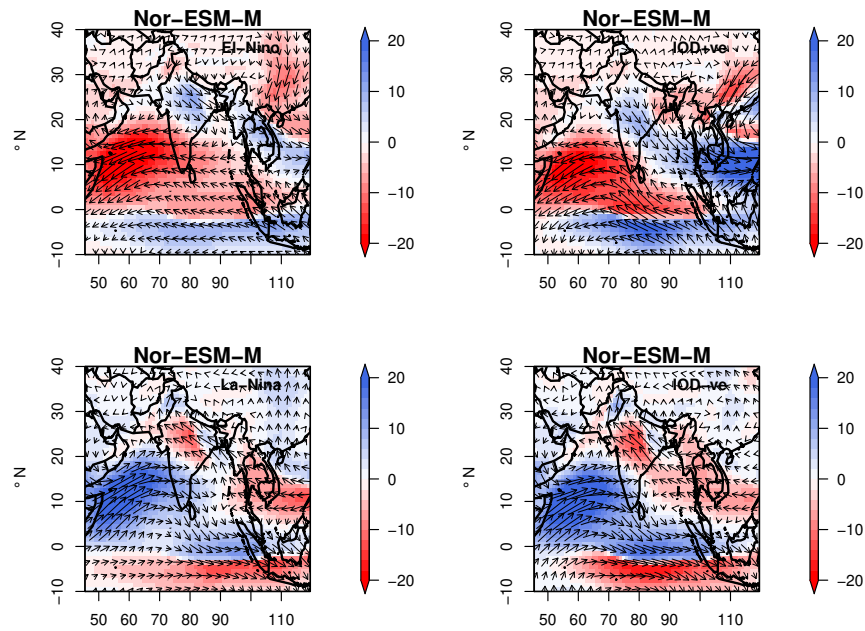


Fig. 10 Moisture flux anomalies (g/kg m/sec) over the Indian subcontinent (JJAS) for El-Niño, La-Niña, positive IOD and negative IOD events observed in Nor-ESM-M GCM for the period of 1951-2005

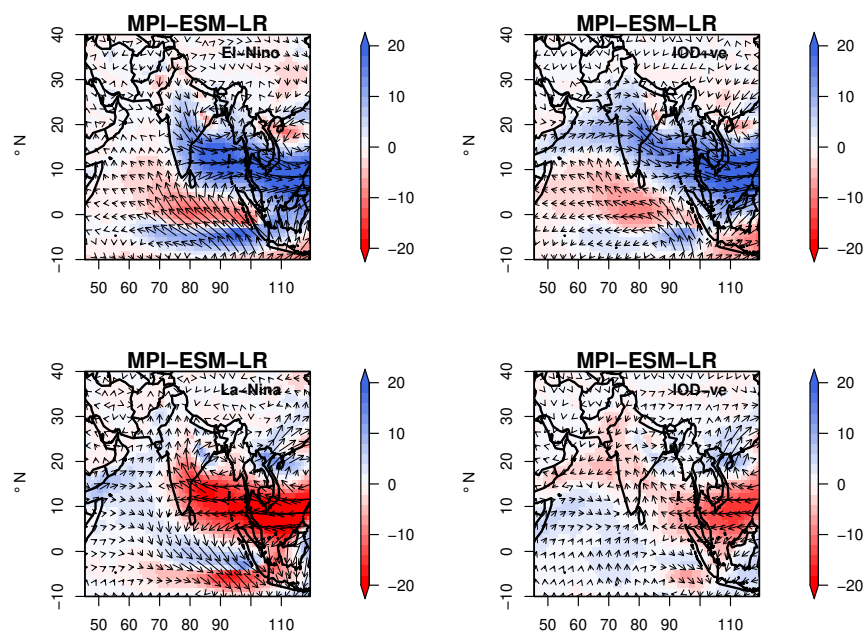


Fig. 11 Moisture flux anomalies (g/kg m/sec) over the Indian subcontinent (JJAS) for El-Niño, La-Niña, positive IOD and negative IOD events observed in MPI-ESM-LR GCM for the period of 1951–2005

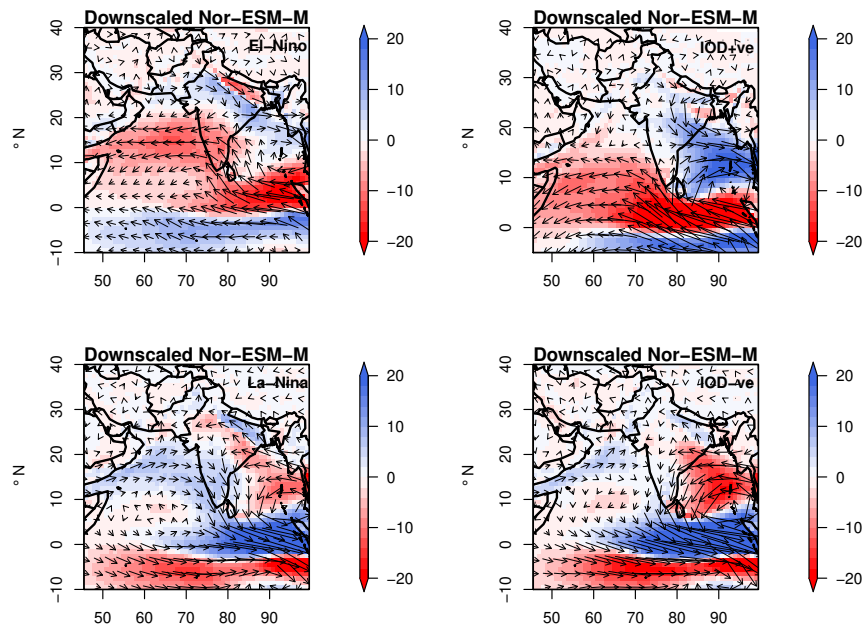


Fig. 12 Moisture flux anomalies (g/kg m/sec) over the Indian subcontinent (JJAS) for El-Niño, La-Niña, positive IOD and negative IOD events observed in downscaled Nor-ESM-M for the period of 1951–2005

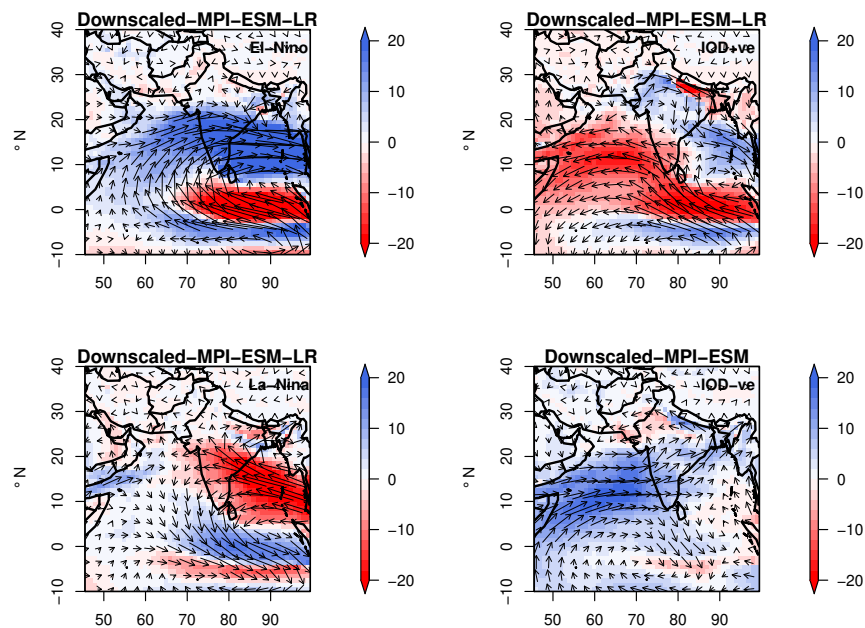


Fig. 13 Moisture flux anomalies (g/kg m/sec) over the Indian subcontinent (JJAS) for El-Niño, La-Niña, positive IOD and negative IOD events observed in downscaled MPI-ESM-LR for the period of 1960-1990

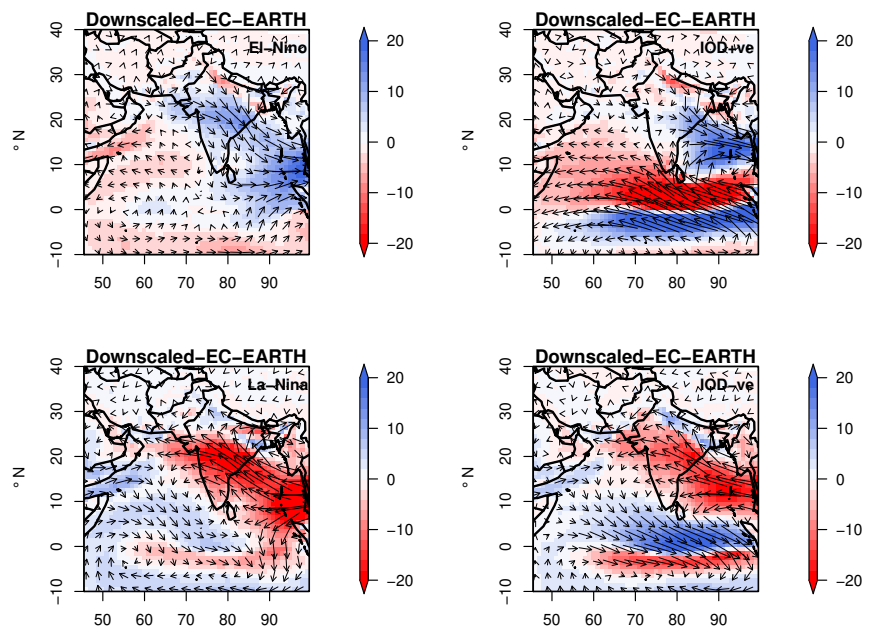


Fig. 14 Moisture flux anomalies (g/kg m/sec) over the Indian subcontinent (JJAS) for El-Niño, La-Niña, positive IOD and negative IOD events observed in downscaled EC-EARTH for the period of 1951-2005